Linear and nonlinear screening effects in two-photon ionization of xenon

Anne L'Huillier
Service de Physique des Atomes et des Surfaces, Centre d'Etudes Nucleaires de Saclay, F-91191 Gif-sur-Yvette Cédex, France

Göran Wendin
Institute of Theoretical Physics, Chalmers University of Technology, S-412 96, Göteborg, Sweden
(Received 9 February 1987; revised manuscript received 15 June 1987)

We apply the random-phase approximation to two-photon ionization. We develop a formalism which, by means of screened electron-photon interactions, includes the nonlinear response and, in particular, double-excitation processes. The theory is illustrated by numerical calculations of the two-photon ionization cross section of the external ($5p$ and $5s$) shell of xenon, over a large energy range: from the two-photon ionization threshold, in the discrete resonance region, and above the one-photon ionization threshold. We show the influence of different many-electron effects, for example, ground-state and final-state correlation, and linear and nonlinear screening. Compared with an independent-electron picture, screening effects lead to a large reduction of the ionization cross section at low photon energy and in contrast, to an important enhancement at higher photon energy, due to the influence of double-excitation and -ionization processes.

I. INTRODUCTION

The interaction of complex atoms with strong fields gives rise to interesting new phenomena which have received considerable attention these last few years. These phenomena are the multiple ionization of rare gases[1-6] and alkaline earths,[7-9] the anomalous behavior of photoelectron spectra in above-threshold-ionization (ATI) experiments,[10] and, as has been recently observed in xenon, the production of high-energy photoemission lines.[11] A rare-gas atom exposed to an intense laser field can absorb an important energy (several hundreds of electron volts) through extremely high-order nonlinear processes.

Several interpretations of multiple multiphoton ionization have been proposed. Some are based upon statistical considerations.[12-15] Others point out the possible role of collective effects at very high laser intensities.[16,17] A major issue is whether the electrons are removed together in a direct processes or one at a time in a sequential process. The present understanding, recently backed up by some photoelectron spectroscopy measurements,[18,19] is that, in most cases, due to the finite rising time of the laser pulse,[20] multiple ionization occurs sequentially, i.e., is actually a succession of one-electron ionization processes. The first ionizations take place and saturate at the beginning of the laser pulse, long before the maximum intensity is reached. As a consequence, the problem comes down to the calculation, or rather estimation of single-ionization probabilities of the different ionic species involved in the transition.[20] Moreover, the experimental data obtained in ion detection[1,2] seem to be consistent, at least for the first ionization steps, with a perturbative picture for the interaction with the radiation field.

The ionization of heavy atoms through the absorption of only one photon is now fairly well described by theories going beyond one-electron approximations, including many-electron effects.[21-26] Unfortunately, the understanding is much more limited for multiphoton ionization processes. Some work has been done on two-electron systems: mostly helium,[27-29] also strontium[30] and recently carbon.[31] The relevant calculations for two- or three-photon ionization of rare gases that we are aware of are those of Pindzola and Kelly[32] in argon, using many-body perturbation theory; Moccia *et al.*[33] in Ar and Ne, using the random-phase approximation (RPA); and McGuire,[34] within a independent-electron approximation. Gangopadhyay *et al.*[35] have applied the multichannel-quantum-defect theory to a calculation of two- and three-photon ionization and autoionization in xenon. Recently, Starace and Jiang[36] have calculated the two-photon ionization cross section of Ar, using a transition-matrix theory. Finally, let us mention some related calculations of the third-order susceptibility of rare gases using the time-dependent local-density approximation.[37,38]

In previous work[28,39-42] we have presented a theoretical description of the interaction of a many-electron atom with an intense laser field, within the framework of diagrammatic many-body perturbation theory. We introduce a screened electron-photon interaction, involving the atomic response and which is described within the random-phase approximation. The theory has been applied to calculations of two-photon ionization of helium[28] and xenon[40] in the zero intensity limit.

In the present paper, we give a full account of the recent work[40] on two-photon one-electron ionization of xenon, and we investigate in greater detail the role of electron screening effects. We go beyond the *linear response*

of the atom to the external field (screening at frequency ω of the first electron-photon interaction) and we investigate the *nonlinear response*: screening of higher harmonics of the field (2ω) and what we call nonlinear screening, screening of all the electron-photon interactions involved in the multiphoton process. This nonlinear screening means the inclusion of double excitation processes, which are found to be very important. We present numerical calculations of two-photon ionization of the $5p$ and $5s$ shell of xenon and we indicate the techniques used for the calculation in the different regions of the spectrum. Let us emphasize that we are interested in the *general behavior* of two-photon ionization over a *broad spectrum,* from the threshold (~ 6 eV) up to much above the ionization limit (19 eV).

In Sec. II, we outline the theoretical formalism for describing two-photon one-electron ionization including screening effects. Section III presents the methods used for calculating the two-photon ionization cross section of the external shell of xenon. The numerical results are presented and discussed in Sec. IV.

II. TWO-PHOTON IONIZATION INCLUDING SCREENING EFFECTS

A theoretical description of multiphoton single ionization including both many-electron and intensity effects has been presented previously.[28] In the present work,[40] we limit ourselves to the lowest order for the radiation field and the two-photon ionization problem, in order to introduce the numerical calculations presented in Sec. IV.

A. Independent-electron approximation

The two-photon one-electron ionization amplitude, diagrammatically represented in Fig. 1(a), is given by the expression

$$t^{a}_{\varepsilon i}(\omega)=\sum_{n}\frac{\langle \varepsilon \mid \mathbf{E}\cdot\mathbf{r} \mid n\rangle\langle n \mid \mathbf{E}\cdot\mathbf{r} \mid i\rangle}{\omega_{ni}-\omega} \ . \tag{1}$$

We are using a one-electron basis set. $|i\rangle$, $|n\rangle$, $|\varepsilon\rangle$ are, respectively, initial-, intermediate-, and final-state orbitals. $-\mathbf{E}\cdot\mathbf{r}$ denotes the electron-photon dipole interaction. ω is the photon energy. $\omega_{ni}=\varepsilon_n-\varepsilon_i$ represent one-electron excitation energies.

This independent-electron approximation cannot give a correct description of the two-photon ionization cross section.[40] Many-electron polarization effects can be included in a simple way by introducing a screened electron-photon interaction, within the framework of the random-phase approximation. After a brief review of this theoretical method, we discuss the different ways of applying it to nonlinear processes.

B. Random-phase approximation

The RPA can be formulated in terms of an effective (screened) electron-photon interaction[21,28,42] $-\mathbf{E}\cdot\mathbf{r}(\omega)$. The diagrammatic perturbation expansion of $-\mathbf{E}\cdot\mathbf{r}(\omega)$ is presented in Fig. 2(a). The first line, which contains the infinite series of forward-propagating bubble diagrams,

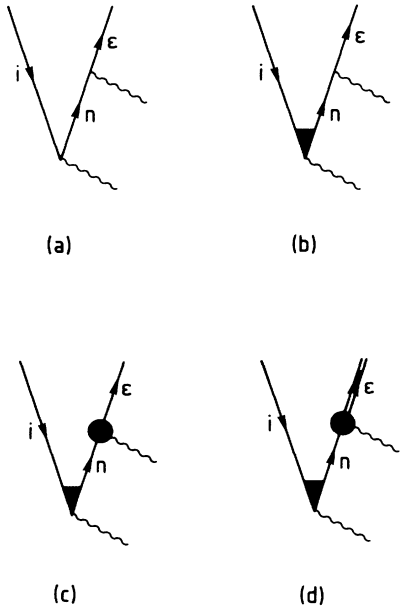

FIG. 1. Diagrammatic representation of the two-photon ionization amplitude: (a) independent-electron approximation; (b) linear response; (c) and (d) nonlinear response (see text).

corresponds to the Tamm-Dancoff approximation (TDA). The RPA also includes ground-state correlation effects, some of which are represented in the second line in Fig. 2(a). We assume, for simplicity, that exchange effects are included in the zeroth-order approximation. The screened electron-photon interaction is the solution of the RPA integral equation [represented in Fig. 2(b)],

$$\mathbf{E}\cdot\mathbf{r}(\omega)=\mathbf{E}\cdot\mathbf{r}-\sum_{n,j}\frac{\langle j \mid 1/r_{12} \mid n\rangle\langle n \mid \mathbf{E}\cdot\mathbf{r}(\omega) \mid j\rangle}{(\omega^2_{nj}-\omega^2)/2\omega_{nj}} \ . \tag{2}$$

$1/r_{12}$ denotes the Coulomb interaction. The expression $\langle j \mid 1/r_{12} \mid n\rangle$ means that an r integration between the $|j\rangle$ and $|n\rangle$ orbitals has been performed.

The RPA represents the *linear response* of the atom. It is equivalent to the linearized time-dependent Hartree theory (the RPAE, random-phase approximation with exchange, being equivalent to the linearized time-dependent Hartree-Fock theory). The effective interaction $-\mathbf{E}\cdot\mathbf{r}(\omega)$ is the sum of the external field $-\mathbf{E}\cdot\mathbf{r}$ and the field induced by the perturbation of the charge density [second term in the left side of Eq. (2)]. The RPA only takes into account the induced field oscillating at the same frequency ω as the external driving field, and not higher harmonics of the field. The question is how this approximation can be extended to multiphoton ionization.

C. Linear response

We shall first describe what we think is the *linear response* of the atomic system to the external field. We take into account the induced *dipole polarization* (induced dipole field oscillating at the same frequency as the driving field). Moreover, apart from virtual double-

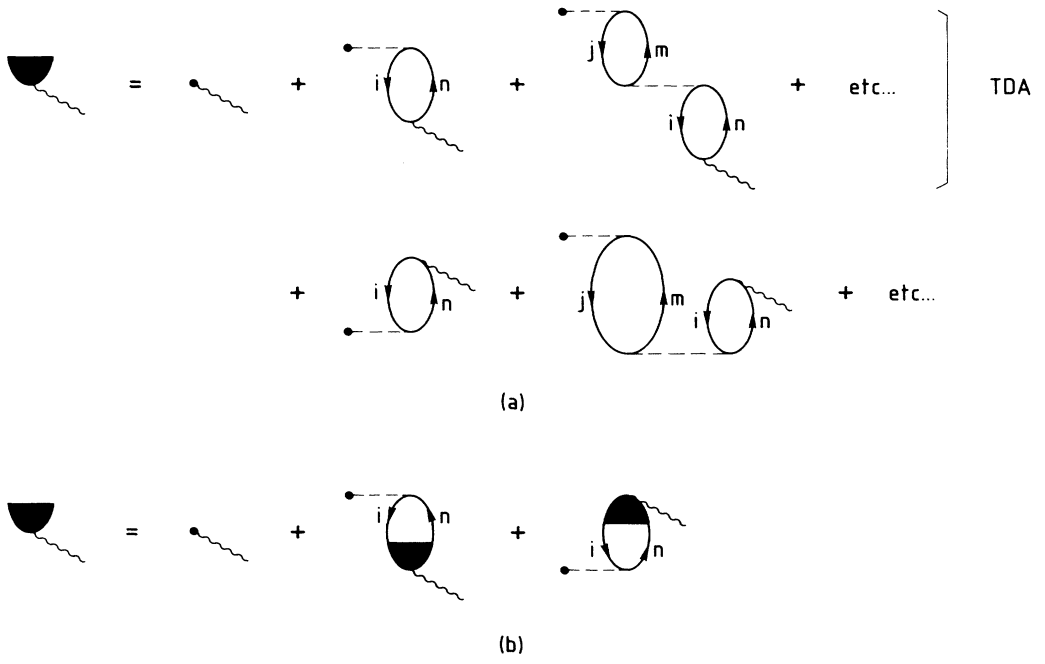

FIG. 2. Random-phase approximation: (a) perturbative expansion, (b) integral equation.

pair excitations in ground and excited states (Fermi sea correlation), we only allow energy-conserving *single-pair excitations* (only one electron can be excited). Figures 3(a)–3(c) show the first-order diagrams (first order in the Coulomb interaction) included within the linear response. The two-photon ionization amplitude, calculated in this approximation can be expressed as

$$t^{b}_{\varepsilon i}(\omega)=\sum_{n}\frac{\langle \varepsilon \mid \mathbf{E}\cdot\mathbf{r} \mid n\rangle\langle n \mid \mathbf{E}\cdot\mathbf{r}(\omega)\mid i\rangle}{\omega_{ni}-\omega}\ . \tag{3}$$

Compared to Eq. (1), we have simply replaced the first electron-photon interaction by the effective electron-photon interaction defined in Eq. (2). A diagrammatic representation of the two-photon amplitude is shown in Fig. 1(b).

D. Nonlinear response (I): Nonlinear screening

So far, the absorption of a second photon does not yield any additional may-electron effects. Going beyond the linear response, we want to describe *polarization effects due to the absorption of two photons.* A first extension of the RPA consists of including multiple electron-hole pair excitations, representing *nonlinear screening.* Two electrons can be simultaneously excited, each absorbing one photon. This double excitation may eventually be energy conserving. The first-order diagrams corresponding to this nonlinear screening in two-photon ionization are drawn in Figs. 3(d)–3(f).

If we neglect the higher-order Coulomb interaction between the electron-hole pair excitations (which then become independent of the state of the system), these processes can be included exactly simply by replacing in Eq. (1) both electron-photon interactions by screened electron-photon interactions [defined in Eq. (2)]. The two-photon ionization amplitude, represented in Fig. 1(c), is given by

$$t^{c}_{\varepsilon i}(\omega)=\sum_{n}\frac{\langle \varepsilon \mid \mathbf{E}\cdot\mathbf{r}(\omega)\mid n\rangle\langle n \mid \mathbf{E}\cdot\mathbf{r}(\omega)\mid i\rangle}{\omega_{ni}-\omega}\ . \tag{4}$$

This approximation overestimates somewhat the screen-

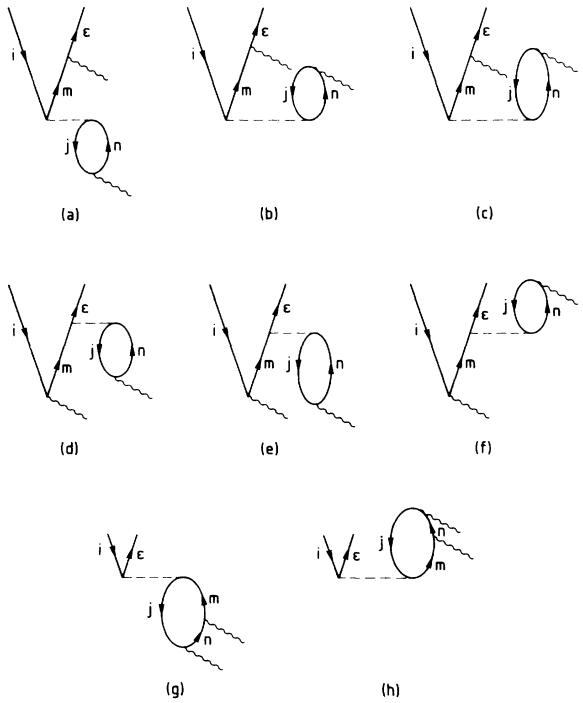

FIG. 3. First-order correlation effects in two-photon ionization (see text).

ing, since it includes exclusion-principle-violating contributions due to neglect of exchange; the second electron-photon absorption is screened in the same away as the first one, although one $5p$ electron has already been excited and does not participate any more to the dynamical screening (more exactly, it participates in a different way). Moreover, this approximation assumes that double-excitation energies are equal to the sum of two one-electron excitation energies ($\omega_{ni}+\omega_{mj}$); we do not take into account the higher-order Coulomb interactions between the electron-hole pair excitations. However, these (electron-hole and hole-hole) monopole interactions should largely cancel each other and the approximation expressed by Eq. (4) should represent a fundamental starting point for describing the average features of two-photon ionization of Xe, in particular below and well above the resonance region.

E. Nonlinear response (II): Screening at higher harmonics

A further extension of the RPA to two-photon ionization consists in describing the induced *monopole and quadrupole polarization*. We add single-pair excitations involving the absorption of two photons (e.g., in Xe, $5p \rightarrow np, nf\ ^1S$ or ^1D). The corresponding first-order diagrams are indicated in Figs. 3(g) and 3(f). This is a linear-screening effect, since only energy-conserving single-pair excitations are taken into account. It describes the atomic response at the second harmonic (2ω) of the laser fundamental frequency. The two-photon ionization amplitude $t^d_{\varepsilon i}(\omega)$, including screening at ω (linear and nonlinear) and screening at 2ω, can be deduced from the system of coupled equations,

$$t^d_{\varepsilon i}(\omega)= t^c_{\varepsilon i}(\omega) - \sum_{n,j} \langle \varepsilon j \mid 1/r_{12} \mid in \rangle \left[\frac{t^d_{nj}(\omega)}{\omega_{nj}-2\omega} + \frac{\overline{t^d_{nj}}(\omega)}{\omega_{nj}+2\omega} \right] , \tag{5a}$$

$$\overline{t^d_{\varepsilon i}}(\omega)= \overline{t^c_{\varepsilon i}}(\omega) - \sum_{n,j} \langle \varepsilon j \mid 1/r_{12} \mid in \rangle \left[\frac{\overline{t^d_{nj}}(\omega)}{\omega_{nj}+2\omega} + \frac{t^d_{nj}(\omega)}{\omega_{nj}-2\omega} \right] , \tag{5b}$$

where $\overline{t^d_{\varepsilon i}}(\omega)$, $\overline{t^c_{\varepsilon i}}(\omega)$ are obtained from $t^d_{\varepsilon i}(\omega)$, $t^c_{\varepsilon i}(\omega)$ by changing ω in $-\omega$ in the energy denominators. This coupled system may be simplified if we assume that ground-state correlation effects [Fig. 3(h)] can be neglected. The two-photon ionization amplitude is then the solution of the integral equation,

$$t^d_{\varepsilon i}(\omega)=t^c_{\varepsilon i}(\omega)- \sum_{n,j} \frac{\langle \varepsilon j \mid 1/r_{12} \mid in \rangle t^d_{nj}(\omega)}{\omega_{nj}-2\omega} . \tag{6a}$$

Another possible approximation, which in contrast overestimates ground-state correlation effects, consists in replacing, in the last term in Eq. (5a), $\overline{t^d_{nj}}(\omega)$ by $t^d_{nj}(\omega)$. System (5) then reduces to

$$t^d_{\varepsilon i}(\omega)=t^c_{\varepsilon i}(\omega)- \sum_{n,j} \frac{\langle \varepsilon j \mid 1/r_{12} \mid in \rangle t^d_{nj}(\omega)}{[\omega^2_{nj}-(2\omega)^2]/2\omega_{nj}} . \tag{6b}$$

These effects represent a contribution much weaker than dipole-polarization effects. As will be explained in Sec. IV, they can be estimated in a simple way by replacing in Eq. (4) the final-state wave function $|\varepsilon\rangle$ by an effective final-state wave function $|\tilde{\varepsilon}\rangle$ according to [Fig. 1(d)]

$$t^d_{\varepsilon i}(\omega)= \sum_n \frac{\langle \tilde{\varepsilon} \mid \mathbf{E}\cdot\mathbf{r}(\omega) \mid n \rangle \langle n \mid \mathbf{E}\cdot\mathbf{r}(\omega) \mid i \rangle}{\omega_{ni}-\omega} . \tag{7}$$

This effective wave function is calculated in a different potential (*LS*-dependent Hartree-Fock) than the initial-state and intermediate-state wave functions (average Hartree-Fock). In this way, screening effects at 2ω are approximately included in the two-photon ionization amplitude.

III. NUMERICAL METHODS

In this section, we describe the methods used for the calculation of the two-photon ionization cross section of the external shell of xenon.

A. One-electron basis set

Most of the calculations presented in this manuscript are performed with a Hartree-Fock (HF) one-electron basis set. The ground-state orbitals are calculated by solving self-consistently the Hartree-Fock equations for the initial state ($5p^6\ ^1S_0$). The excited orbitals are calculated from a frozen HF potential which can be built in many ways,[43] as discussed in detail in the Appendix. The potential that we use for the calculation of the two-photon ionization cross section of xenon has the following properties: the self-interaction is removed from the Coulomb part of the potential, but not from the exchange (see Appendix for more detail). In the case of intermediate excited states ($5p^{-1}ns$, $5p^{-1}nd$, and $5s^{-1}np$), we also include the complete ladder (intrachannel) interaction in the potential. As a consequence, an RPA calculation (i.e., only bubble diagrams and no ladders) based upon this potential is nearly equivalent to the more common RPAE (RPA with exchange) treatment, based upon a V^{N-1} type of potential. In this way, exchange effects are included in the zeroth-order approximation.

For comparison, we shall also present some results obtained with a local-density approximation (LDA) basis set.[28,40] Except in the region of resonances of excited states, described in average in the local-density approximation,[40] an RPA calculation for the two-photon ionization cross section, based upon our HF basis set (RPAE) or based upon a LD basis (LDRPA) should yield similar results and it appeared to us worth comparing both approaches.

B. Two-photon ionization cross section

The two-photon $5p$-shell ionization generalized cross section σ_2 expressed in $\mathrm{cm}^4\,\mathrm{s}$ can be written as

$$\sigma_2 = 2\pi(\alpha c/a_0)(1/FF_0)^2 \sum_{l_\varepsilon} |t_{\varepsilon i}(\omega)|^2 , \quad (8)$$

where α is the fine-structure constant, c the speed of light, and a_0 the Bohr radius. F is the laser flux in photons/cm^2 s. $F_0 = 3.22\times10^{34}$ photons/cm^2 s. $i = 5p$ is the initial state (a summation over the number of electrons of the $5p$ shell is understood). $\varepsilon = \varepsilon p$ or εf is the final state (l_ε is its orbital quantum number). After separation of angular and radial variables, the partial amplitudes $t_{\varepsilon i}(\omega)$ are given by

$$t_{\varepsilon i}(\omega) = F\omega \sum_n C(\varepsilon,n,i) \frac{\langle \varepsilon | R_2 | n \rangle \langle n | R_1 | i \rangle}{\omega_{ni} - \omega} . \quad (9)$$

$C(\varepsilon,n,i)$ are coefficients accounting for the spin summation and the angular integration. Depending on the approximation chosen for including screening effects, $R_1, R_2 = r, r(\omega)$. For $5p \rightarrow \varepsilon f$ transitions, there is only one channel $5p \rightarrow d \rightarrow f$. $|n\rangle = |nd\rangle$ in Eq. (9) and the summation is performed over the discrete ($5d, 6d, \ldots$) and continuum spectrum. In the case of $5p \rightarrow \varepsilon p$ transitions, two channels $5p \rightarrow d \rightarrow p$ and $5p \rightarrow s \rightarrow p$ interfere and the corresponding amplitudes must be added. The summation over n in Eq. (9) is a double summation over $|ns\rangle$ and $|nd\rangle$ intermediate states.

The two-photon ionization amplitude [Eq. (9)] is calculated by applying the perturbed-orbital method. We build the perturbed orbital,

$$|\tilde{\omega}\rangle = \sum_n C(\varepsilon,n,i) \frac{|n\rangle\langle n | R_1 | i\rangle}{\omega_{ni} - \omega} , \quad (10)$$

by explicitly summing over intermediate states. Implicit-summation techniques are usually preferred in similar calculations. However, the explicit summation presents the advantage of being much more flexible for the description of screening effects [$R_1 = r(\omega)$]. For example, a resonant state requiring a "special" treatment (see Sec. III C) can be easily isolated from Eq. (10). In the HF approximation, we sum over ten discrete states (up to $14d$ or $15s$), we integrate in the continuum from 0.002 to 20 Ry (90 energy points), and we approximate the remaining summation over Rydberg states and the integration from 0 to 0.002 Ry using an interpolation method. In the local-density approximation, the summation is reduced to continuum states (about 70), since there are no excited bound states.

The two-photon ionization amplitude is then equal to

$$t_{\varepsilon i}(\omega) = \langle \varepsilon | R_2 | \tilde{\omega} \rangle . \quad (11)$$

The calculation of this matrix elements does not present any difficulty, except for above-threshold ionization processes. When the photon energy is higher than the ionization energy, the perturbed orbital [Eq. (10)] exhibits the behavior of a continuum wave function and (11) is a free-free matrix element. The technique for calculating these matrix elements has been described in detail elsewhere.[28,44] It consists in first integrating numerically from zero to a cutoff point r_c and then estimating the remaining integration from r_c to infinity using the analytical asymptotic form of the continuum wave functions. Let us point out that the best accuracy is reached when r_c is as near as possible from the core region (typically 30 a.u. in Xe). It is then essential to get very good asymptotic developments, valid at small distances.

C. Effective electron-photon interaction

The effective field $r(\omega)$ satisfies the integral equation [Eq. (2)]

$$r(\omega) = r - \sum_{n,j} \frac{C_{nj} Y^1_{jn}(r) \langle n | r(\omega) | j \rangle}{(\omega^2_{nj} - \omega^2)/2\omega_{nj}} , \quad (12)$$

with, in both RPAE and LDRPA calculations,

$$C_{nj} = \frac{2(2l_j+1)(2l_n+1)}{3} \begin{bmatrix} l_j & 1 & l_n \\ 0 & 0 & 0 \end{bmatrix}^2 . \quad (13)$$

The matrix elements in Eq. (12) are radial matrix elements. In particular, $Y^1_{jn}(r)$ represents the radial part of $\langle j | 1/r_{12} | n \rangle$. Equation (12) is solved by means of a Fredholm approximation,

$$r(\omega) = r - \sum_{n,j} \frac{C_{nj} Y^1_{jn}(r) \langle n | r | j \rangle}{(\omega^2_{nj} - \omega^2)/2\omega_{nj}} / \epsilon(\omega) , \quad (14)$$

with

$$\epsilon(\omega) = 1 + \sum_{n,j} \frac{C_{nj} V_{njjn}}{(\omega^2_{nj} - \omega^2)/2\omega_{nj}} . \quad (15)$$

$V_{njjn} = \langle n | Y^1_{jn} | j \rangle$ is the radial part of the Coulomb matrix element $\langle nj | 1/r_{12} | jn \rangle$. Although this approximation is good enough in the case of one channel, it must be carefully applied when several channels are mixed. Let us call $\epsilon_c(\omega)$ the solution of Eq. (15) for a channel (c). The effective field is approximated by

$$r(\omega) = r - \sum_{(c)} \left[\sum_{(n,j)\in(c)} \frac{C_{nj} Y^1_{jn}(r) \langle n | r | j \rangle}{(\omega^2_{nj} - \omega^2)/2\omega_{nj}} \frac{1}{\epsilon_c(\omega)} \right] . \quad (16)$$

It means that each infinite series of bubbles (e.g., in Fig. 2) contains one type of interaction. Interchannel coupling is realized only to first order. In the neighborhood of a resonance, however, interchannel mixing becomes important and requires a better treatment, going beyond the first order.[21] Denoting $i \rightarrow d$ the resonant transition (e.g., in Xe $5p \rightarrow 6s$), we define $\bar{r}(\omega)$, $\bar{Y}^1_{id}(r,\omega)$, respectively represented in Figs. 4(a) and 4(b) by

$$\bar{r}(\omega) = r - \sum_{(n,j)\,[\neq(d,i)]} \frac{C_{nj} Y^1_{jn}(r) \langle n | \bar{r}(\omega) | j \rangle}{(\omega^2_{nj} - \omega^2)/2\omega_{nj}} , \quad (17)$$

$$\bar{Y}^1_{id}(r,\omega) = Y^1_{id}(r) - \sum_{(n,j)\,[\neq(d,i)]} \frac{C_{nj} Y^1_{jn}(r) \langle n | \bar{Y}^1_{id}(r,\omega) | j \rangle}{(\omega^2_{nj} - \omega^2)/2\omega_{nj}} . \quad (18)$$

The effective field $r(\omega)$, represented in Fig. 4(c), is given by

$$r(\omega) = \bar{r}(\omega) - \frac{C_{di} \bar{Y}^1_{id}(r,\omega) \langle d | \bar{r}(\omega) | i \rangle}{(\omega^2_{di} - \omega^2)/2\omega_{di} + C_{di} \bar{V}_{dd}(\omega)} , \quad (19)$$

with $\bar{V}_{dd}(\omega) = \langle d | \bar{Y}^1_{id}(r,\omega) | i \rangle$. In the same way, the two-photon ionization amplitude [Fig. 4(d), with $R_2 = r$] is given by

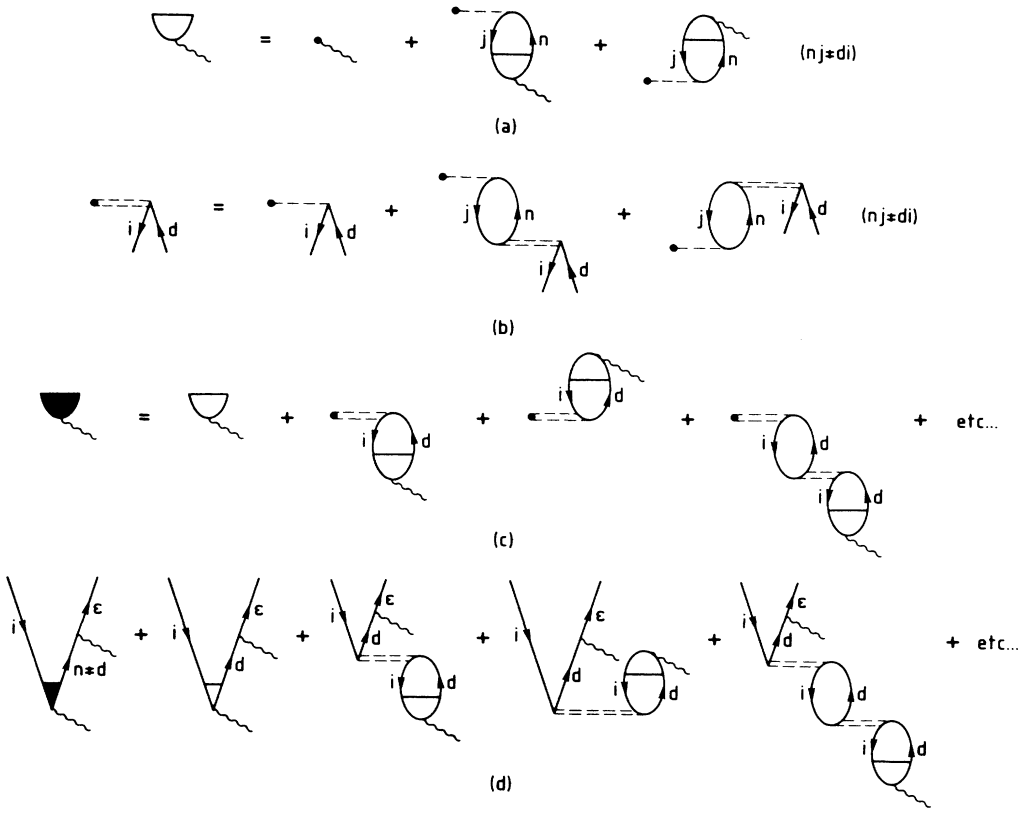

FIG. 4. Resonant two-photon ionization: (a) $\bar{r}(\omega)$, (b) $\bar{Y}^{1}_{id}(r,\omega)$, (c) $r(\omega)$, (d) renormalization of the two-photon ionization amplitude.

$$t_{\varepsilon i}(\omega)=\sum_{n\,(\neq d)} C(\varepsilon,n,i)\frac{\langle \varepsilon \mid R_2 \mid n\rangle\langle n \mid r(\omega)\mid i\rangle}{\omega_{ni}-\omega}+C(\varepsilon,d,i)\frac{\langle \varepsilon \mid R_2 \mid d\rangle\langle d \mid \bar{r}(\omega)\mid i\rangle}{\omega_{di}-\omega+C_{di}\bar{V}_{dd}(\omega)2\omega_{di}/(\omega_{di}+\omega)} . \tag{20}$$

It is divided in two parts: off resonant [first term on the right side of Eq. (20); first diagram in Fig. 4(d)] and resonant [second term on the right side of Eq. (20); the sum of the last four diagrams in Fig. 4(d)]. This renormalization is quite similar to the treatment of resonant two-photon ionization including strong-field effects (absorption and reemission of photons). However, the correction term in the denominator in Eq. (20) does not depend on the laser intensity. Moreover, it is *real*. The Coulomb interaction induces a *shift* of the resonance but, as long as ω_{di} is lower than the binding energy of electron i, does not broaden it. (The two-photon ionization amplitude still becomes infinite at some energy value.)

In Fig. 5 we have plotted the variation of the effective field $r(\omega)$ as a function of r for different (off-resonant) photon energies from 0.3 up to 1.5 Ry (see Ref. 26). The effective field is calculated with local-density wave functions by including the interaction with most of the external subshells ($3d$,$4s$,$4p$,$4d$,$5s$,$5p$), the dominant one being, of course, the $5p$ subshell. Above the LD-ionization threshold (0.62 Ry), $r(\omega)$ becomes complex and the effective field plotted in Fig. 5 is the real part of $r(\omega)$. The effective field is generally lower than the external field (r, materialized by the straight line with slope 1), except at high photon energy. The external field is screened out of the outermost shell and this screening will induce a reduction of the cross section compared to an independent-electron picture.[28,39]

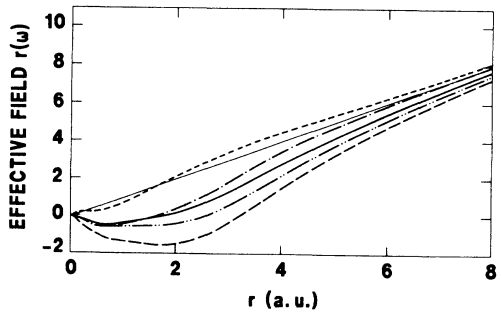

FIG. 5. Effective field $r(\omega)$ as a function of r (in a.u.). (——), 0.31 Ry; (–··–··–··–), 0.6 Ry; (– – –), 0.7 Ry; (—·—·—·), 1 Ry; (-----), 1.5 Ry. Above 0.62 Ry, the real part of $r(\omega)$ is plotted.

IV. NUMERICAL RESULTS

A. Two-photon ionization of the 5p subshell

Figures 6 and 7 show the two-photon $5p$-shell ionization spectrum of Xe, for linearly polarized light, calculated with different approximations. The solid line is the independent-electron (HF) approximation. The dashed line is the result of an RPAE calculation including nonlinear screening [Eq. (4), Fig. 1(c)]. The dotted line is the result of a similar calculation performed with a local-density basis set (LDRPA). The cross in Fig. 6 is an experimental result obtained by McCown *et al.*[45] at 193 nm (0.47 Ry). Finally, the squares plotted in Fig. 6 refer to a calculation of McGuire, using a Hartree-Fock-Slater type of basis and Green's-function techniques[34] and the solid circles to a calculation of Gangopadhyay *et al.*,[35] using multichannel quantum-defect theory. For this latter calculation, we have represented the results above the second ionization limit and added the contributions of the final ionic cores $P_{1/2}, P_{3/2}$. The ordinates scale in Figs. 6 and 7 is logarithmic and covers several orders of magnitude; differences between the cross sections are therefore very significant. The photon energy is varied from the two-photon HF ionization threshold (0.46 Ry) up to 0.86 Ry in Fig. 6, scanning the first excited levels $5p^5 6s, 5d, 7s, 6d, 8s$ and then in Fig. 7 from 0.98 Ry to 1.40 Ry, describing an ATI (above-threshold-ionization) process.

In the threshold region, screening effects lead to a large reduction of the two-photon ionization cross section compared to the independent-electron approximation. The *(ab initio)* results obtained within the RPAE (or LDRPA) are in good agreement with the results of Gangopadhyay *et al.*,[35] using multichannel-quantum-defect theory. In this latter calculation, energy levels and oscillator strengths are taken to be experimental;

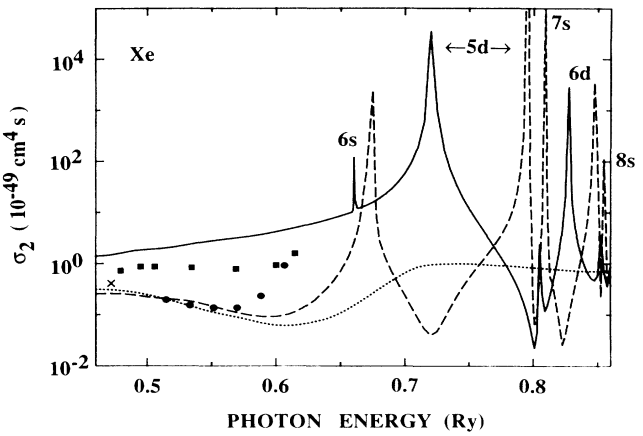

FIG. 6. Two-photon ionization cross section of the $5p$ shell of Xe. (——), Hartree-Fock independent-electron approximation; (— — —), RPAE nonlinear screening; (· · · ·), LDRPA nonlinear screening; (■), independent-electron result obtained by McGuire (Ref. 34); (●), MQDT result obtained by Gangopadhyay *et al.* (Ref. 35); (×), experimental point at 193 nm by McCown *et al.* (Ref. 45).

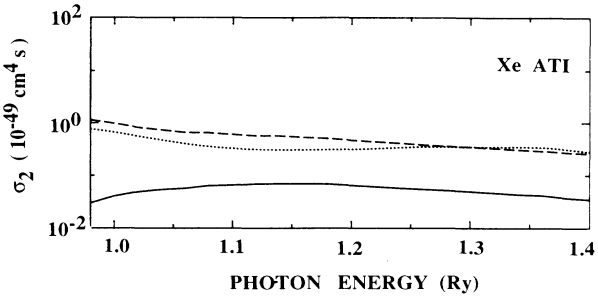

FIG. 7. Above-threshold ionization (same notations as in Fig. 6).

screening effects should be implicitly included in this approach. In contrast, the calculation performed by McGuire[34] yields a two-photon ionization cross section, which, in the threshold region, is higher than the RPAE result by more than a factor of two. Our HF basis set is rather technical and chosen so that the RPA treatment based upon it (bubble diagrams only) is as accurate as possible. We have performed a similar independent-electron calculation using a more physical one-electron basis set (based upon a self-interaction free V^{N-1} HF potential). We then obtained good agreement with McGuire's results.

The RPAE screening leads to an important shift of the $5p^{-1}nd$ resonances towards higher energies (Fig. 6) and to a redistribution of the strength of the $5p^{-1}ns$ and $5p^{-1}nd$ resonances. Moreover, the resonances show up in the partial cross sections. This is due to channel mixing introduced by the screening (see Sec. III C). In this energy region, the LDRPA calculation (dotted line) gives an average description of the real two-photon ionization spectrum. (The LD $5p$-ionization energy is equal to 0.62 Ry and there are no bound excited states.)

Finally, above the ionization threshold (Fig. 7), the two-photon ionization cross section is considerably enhanced compared to the independent-electron result, by more than one order of magnitude. This is due to *antiscreening* effects (enhancement of the effective field, as shown in Fig. 5 for $\omega > 1$ Ry) and *double ionization* processes. The main contribution to the two-photon ionization amplitude comes from the imaginary part of $r(\omega)$ in both electron-photon interactions [Eq. (4)]. This means that two photons are separately absorbed (energy conservation) by two different electrons. This double ionization is followed by autoionization [see Figs. 3(d) and 3(e)].

In this calculation, we neglect the spin-orbit interaction of the $5p^5$ core. In reality, Xe has two ionization limits $^2P_{3/2}$, $^2P_{1/2}$, separated by about 0.1 Ry (0.89, 0.99 Ry). This approximation has two consequences. First, we cannot describe two-photon autoionization processes [represented in Fig. 8(a)] taking place between the ionization thresholds (i.e, below 0.5 Ry in Fig. 6).[35] Second, the energies of the excited states calculated by means of the RPAE and indicated in Fig. 6 by the positions of the resonances must be considered as an average over the different configurations of the core. The disagreement

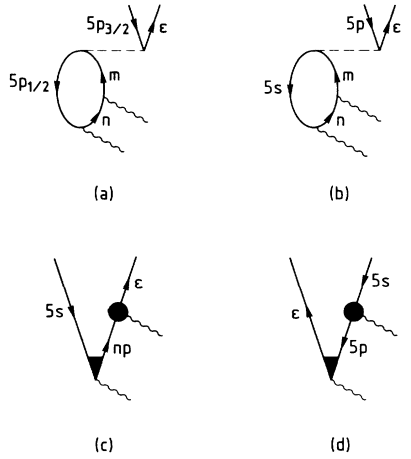

FIG. 8. (a) Autoionization due to the spin-orbit interaction of the ionic core, (b) autoionization following the excitation of a 5*s* electron, (c) and (d) ionization of a 5*s* electron.

between our result and the one obtained by Gangopadhyay *et al.*[35] at high photon energy (≥ 0.60 Ry) is merely due to the fact that we use our calculated nonrelativistic value for the position of the $5p^5(^2P_{3/2})6s\,^1P_1$ resonance (experimental energy, 0.62 Ry). A better agreement would probably be obtained if the spin-orbit interaction were properly included. However, in the present work, we are interested in the *general features* of the two-photon ionization spectrum over a large energy domain, and we shall deal with the problem of including the spin-orbit interaction in multiphoton ionization in a latter work.

B. Two-photon ionization of the 5*s* subshell

The influence of the 5*s* subshell in two-photon ionization of xenon is twofold. First, there are autoionization resonances due to two-photon excitation of a 5*s* electron, as shown in Fig. 8(b). These autoionization processes would modify the two-photon ionization spectrum in the region 0.82 Ry $<\omega<0.94$ Ry by introducing additional resonances. Second, above the two-photon 5*s*-ionization threshold (0.94 Ry), the ionization of a 5*s* electron becomes possible. The two-photon ionization amplitude is the sum of two contributions [represented in Figs. 8(c) and 8(d)] which differ by the position of the initial hole, in the 5*s* shell [Fig. 8(c)] or in the 5*p* shell [Fig. 8(d)]. Both contributions can easily be summed and the 5*s*-ionization amplitude (in the nonlinear screening approximation) is written as

$$t_{\varepsilon i}(\omega)=F\omega \sum_{n=5p,6p,\ldots} \frac{\langle \varepsilon \mid r(\omega) \mid n \rangle \langle n \mid r(\omega) \mid i \rangle}{\omega_{ni}-\omega}, \tag{21}$$

with $i=5s$, $n=np$. The summation is performed in the discrete spectrum including the 5*p* state and in the continuum spectrum. $r(\omega)$ includes, of course, contributions from the 5*p* and 5*s* shells. The 5*s*-ionization partial cross section starts at 0.94 Ry and presents a pronounced maximum at about 0.97 Ry. The total ionization cross section is shown in Fig. 9 (from 0.98 Ry) together with the 5*p*-ionization partial cross section (Fig. 7). Again, the HF result in solid line (5*p* ionization) and in dot-dashed line (5*p* + 5*s* ionization) is compared to the RPAE result in dashed line (5*p*) and in dotted line (5*p* + 5*s*). Apart from the 5*s*-threshold region, the contribution of the 5*s* ionization to the total cross section remains very weak. This is especially true when screening effects are included, as could have been intuitively expected; a 5*s* electron is screened out from the external perturbation by the 5*p* shell, so that the influence of 5*s* ionization is reduced.[28,39]

C. Influence of polarization and correlation effects

In this section, we investigate the influence of polarization and correlation effects in two-photon ionization of the 5*p* shell of Xe. We vary the amount of screening (linear, nonlinear, etc.) included in the RPA and we study the influence of ground-state correlation effects. We want to estimate the relative importance of the different many-electron effects represented in Fig. 3. Figures 10 and 11 show the two-photon ionization cross section in the discrete and continuum regions calculated within different approximations.

1. Linear and nonlinear screening effects

The solid line is the result shown previously in Figs. 6 and 7, obtained by screening both electron-photon interactions [Eq. (4), Fig. 1(c)]. The dot-dashed line is obtained within the linear response, by screening only the first electron-photon interaction [Eq. (3), Fig. 1(b)]. The comparison between these results demonstrates the importance contribution of nonlinear screening effects. They induce a reduction of the cross section at low photon energy, up to a factor of 4 at 0.6 Ry. In contrast, the cross section is enhanced in the discrete resonance region and above the ionization threshold (Fig. 11) (i.e., when double excitation processes become energy conserving). The widths and strengths of the resonances in Fig. 10 strongly increase and the line shapes change when the second electron-photon interaction is screened, i.e., when double excitations are included. However, due

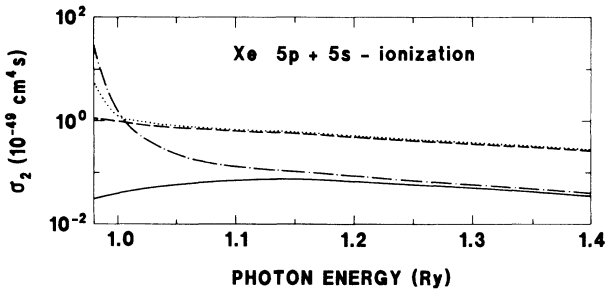

FIG. 9. Total two-photon ionization of the external shell of Xe. (—·—·—·), HF independent-electron approximation; (· · · ·), RPAE nonlinear screening; (——), 5*p* ionization, HF; (— — —), 5*p* ionization, RPAE (same as in Fig. 7).

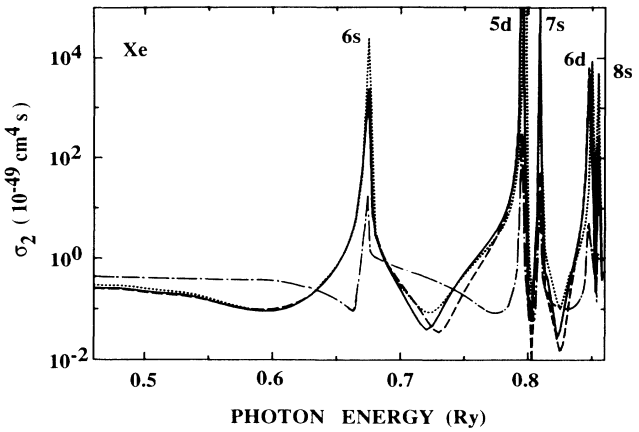

FIG. 10. (——), RPAE nonlinear screening; (—·—·—·), RPAE linear screening; (· · · ·), TDAE nonlinear screening (no ground-state correlation effects); (— — —), RPAE screening at ω and 2ω.

to the approximation made in Eq. (4) (independence of electron-hole pair excitations), the contribution of these double-excitation processes may be somewhat overestimated. In particular, in this approximation, double-excitation resonances coincide with single-excitation resonances. If the Coulomb shift were included, the double-excitation resonances would be displaced to more realistic double-excitation energies.

2. *Ground-state correlation effects*

The dotted line in Figs. 10 and 11 is obtained by neglecting dipole ground-state correlation effects [Figs. 3(b) and 3(c)]. The two-photon ionization amplitude is evaluated according to Eq. (4), with an effective electron-photon interaction $r(\omega)$ calculated within the Tamm-Dancoff approximation (we keep only forward-propagating bubbles in Fig. 2),

$$r(\omega)=r-\sum_{n,j}\frac{C_{nj}Y^1_{jn}(r)\langle n\mid r(\omega)\mid j\rangle}{\omega_{jn}-\omega}\ . \tag{22}$$

Apart from a slight shift of the resonances, ground-state correlation effects seem to affect mainly the high-energy region (Fig. 11); the cross section is lowered by a factor of about 3 at 1.4 Ry when these effects are included. Note that we agree quite well with the conclusion of Pindzola and Kelly[32] and Starace and Jiang[36] about the influence of correlation effects in two-photon ionization of argon. In both calculations in Ar and Xe, the correction induced by ground-state correlation effects in the discrete spectrum amounts to about 20–30%. This can barely be seen in Fig. 10, due to the logarithmic scale; we are interested in much more important effects such as double-excitation processes which may enhance (or reduce) the cross section by more than one order of magnitude.

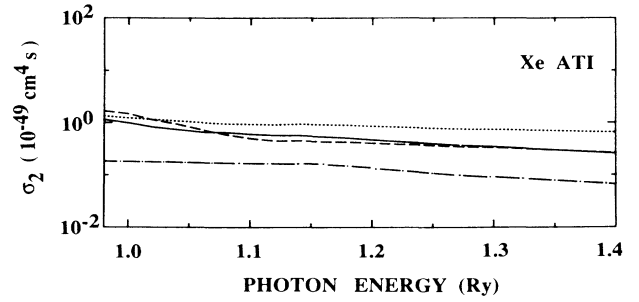

FIG. 11. ATI (same notations as in Fig. 10).

3. *Final-state correlation effects (screening at 2ω)*

Finally, the dashed line in Figs. 10 and 11 is an approximate calculation including nonlinear screening and screening at 2ω. The two-photon ionization amplitude is calculated as in Eq. (7); the wave function $|\varepsilon f\rangle$ is replaced by an effective wave function $|\varepsilon f\,{}^1D\rangle$ calculated from a HF LS-dependent potential (see Appendix). We have not done the same approximation for final $|\varepsilon p\rangle$ states, since we would have had to select either the $|\,{}^1S\rangle$ or $|\,{}^1D\rangle$ component (no mixing is possible). However, the dominant ionization channel is $5p\rightarrow d\rightarrow f$, and the most important effects should be included. The result obtained, shown by the dashed line in Figs. 10 and 11 shows that these final-state correlation effects are indeed not very important; the dashed and solid lines are nearly on top of each other except in the critical antiresonance regions and in the low-energy part in Fig. 11.

D. Influence of screening in above-threshold ionization

As we have calculated the two-photon ionization cross section when the photon energy is greater than the ionization energy, it is of interest to compare the probabilities between one-photon ionization and two-photon ionization. We have then calculated the one-photon ionization cross section σ_1 (Mb),

$$\sigma_1=4\pi^2\alpha a_0^2\omega\sum_{l_\varepsilon}C_{\varepsilon i}\mid\langle\varepsilon\mid R_1\mid i\rangle\mid^2\ . \tag{23}$$

We use the same notations as before. $R_1=r$ within the independent-electron approximation; $R_1=r(\omega)$, given by Eq. (12), within the random-phase approximation. In Fig. 12, the ratio σ_2F/σ_1 ($F=10^{33}$ photons/cm^2 s) is

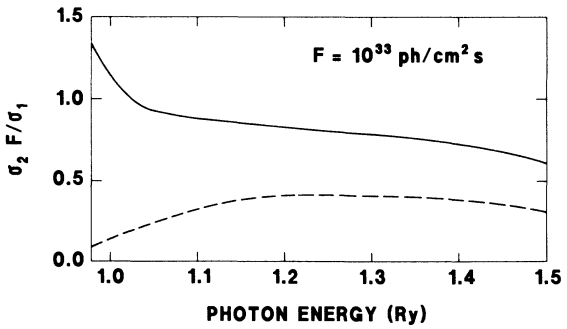

FIG. 12. Plot of the ratio σ_2F/σ_1 as a function of the photon energy. $F=10^{33}$ photons/cm^2 s. (——), RPAE nonlinear screening result; (— — —), independent-electron approximation.

plotted as a function of the photon energy ω from 0.98–1.50 Ry. The solid line is the RPAE result [σ_2 is calculated by including nonlinear screening, as in Eq. (4), Fig. 1(c)]. The dashed line is the independent-electron result. Physically, $\sigma_2 F/\sigma_1$ represents the ratio between the intensities of the second and first photoelectron peaks, if we assume that the laser pulse is square both in time and space. This result illustrates again the importance of nonlinear screening effects in two-photon above-threshold ionization of Xe. Ionization occurs essentially via a doubly excited intermediate state, which recombines.

V. CONCLUSION

We demonstrate that the linear response is not appropriate for describing the dynamics of a two-photon ionization process. One needs to go beyond it and to incorporate the *nonlinear response:* screening at higher harmonics of the laser field and especially nonlinear screening, i.e., screening of all the electron-photon interactions involved in the multiphoton process. These ideas are supported by a number of numerical calculations performed in xenon, over an extended spectrum; from the two-photon ionization threshold (0.46 Ry) up to 1.4 Ry, above the one-photon ionization threshold.

We compare different basis sets, local-density approximation and Hartree-Fock, and we obtain a good agreement between the LD-based and HF-based spectra over a large energy range, except in the discrete resonance region, where the LDA (or LDRPA) gives an average cross section. We calculate the 5*s*-ionization cross section and we show that the influence of the 5*s* subshell on the total ionization cross section is very weak; this is mainly due to screening by the other external electrons. Finally, we discuss in great detail the influence of different many-electron effects, such as ground- and final-state correlation, linear and nonlinear screening.

Linear and nonlinear *dipole polarization* effects [Figs. 3(a), 3(d) and 3(e)] are absolutely essential for describing properly the dynamics of a two-photon ionization process. Although linear-screening effects have been considered before[32,33] (by using a HF *LS*-dependent basis set), as far as we can find, this is one of the first calculations[36,40] going beyond the linear response and including in an approximate way double-excitation processes [Figs. 3(d) and 3(e)]. This is done by means of an effective electron-photon interaction, which must replace *everywhere* the dipole operator in the usual independent-particle treatment of multiphoton ionization. At low photon energy, both linear and nonlinear screening effects lead to a considerable reduction of the two-photon ionization cross section compared to an independent-particle approximation. In contrast, the cross section is enhanced at higher photon energy, due to double-excitation processes. The photons are initially absorbed by two *different* electrons. The importance of these nonlinear screening effects shows that it would be of the greatest interest to refine the present calculations by including the higher-order Coulomb interaction between the double electron-hole pair excitations and by taking care of the exchange effects. This would allow us to get a more realistic spectrum in the high-energy region.

ACKNOWLEDGMENTS

One of us (A.L.) acknowledges the hospitality of Chalmers University of Technology. This work has been supported by the Swedish Natural Science Research Council.

APPENDIX

In this appendix, we present different frozen Hartree-Fock potentials which can be chosen for calculating the excited orbitals (from the 5*p* shell). In Figs. 13(a)–13(d), we have represented all the diagrams involving the $5p \rightarrow nl\ ^1L$ intrachannel interaction. The contributions of these diagrams for the different channels involved (including also the $5s \rightarrow nl\ ^1L$ channels) are indicated in Table I. Columns (a) and (b) are direct interaction terms; R^k denotes the Slater integral $R^k(5pnl, 5pn'l)$ or $R^k(5snl, 5sn'l)$. Columns (c) and (d) represent exchange terms; $R^k = R^k(5pnl, n'l5p)$ or $R^k(5snl, n'l5s)$. We distinguish the monopole (b_0) and quadrupole (b_2) parts of the ladder interaction, represented by Fig. 13(b). In the following, we shall denote by (a)–(d) the contributions of the diagrams represented in Figs. 13(a)–13(d), or, *equivalently,* the terms reported in columns (a)–(d) in Table I for each transition. Different choices for the potential can be contemplated, depending how much of the intrachannel interaction we want to include in the zeroth-order approximation (in the single-particle basis set). The usual Hartree-Fock (V^N) approximation is such that

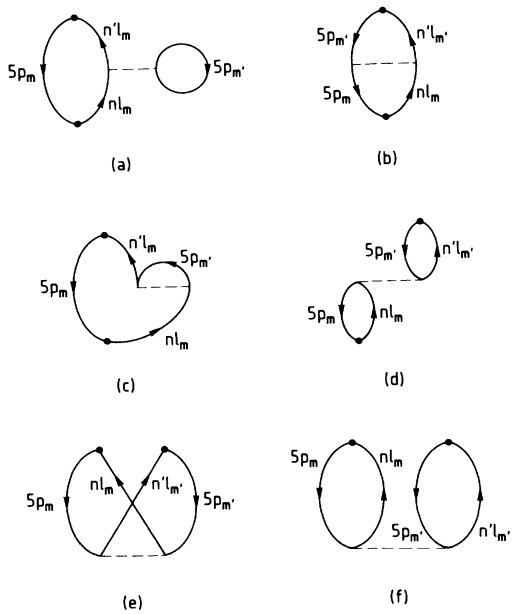

FIG. 13. (a)–(d) diagrammatic representation of $5p \rightarrow nl\ ^1L$ intrachannel interactions; (e),(f) ground-state correlation effects. The dot denotes the interaction with the radiation field (absorption of one photon for $5p^{-1}nl\ ^1P$ states, two photons for $5p^{-1}nl\ ^1D$ or ^1S states).

TABLE I. Contributions of $5p^{-1}nl\ ^1L$ and $5s^{-1}nl\ ^1L$ intrachannel interactions. (a), (b), (c), (d) refer to diagrams (a), (b), (c), (d), in Fig. 13. R^k ($k=0$–4) is the Slater integral $R^k(5pnl,5pn'l)$ or $R^k(5snl,5sn'l)$ in columns (a) and (b); $R^k=R^k(5pnl,n'l5p)$ or $R^k(5snl,n'l5s)$ in columns (d) and (c).

	(a)	(b)	(c)	(d)
$5p\rightarrow ns\ ^1P$	$6R^0$	$-R^0$	$-R^1$	$\frac{2}{3}R^1$
$5p\rightarrow nd\ ^1P$	$6R^0$	$-R^0-\frac{1}{5}R^2$	$-\frac{2}{5}R^1-\frac{9}{35}R^3$	$\frac{4}{3}R^1$
$5p\rightarrow np\ ^1S$	$6R^0$	$-R^0-\frac{2}{5}R^2$	$-R^0-\frac{2}{5}R^2$	$6R^0$
$5p\rightarrow np\ ^1D$	$6R^0$	$-R^0-\frac{4}{25}R^2$	$-R^0-\frac{2}{5}R^2$	$\frac{12}{25}R^2$
$5p\rightarrow nf\ ^1D$	$6R^0$	$-R^0-\frac{4}{25}R^2$	$-\frac{9}{35}R^2-\frac{4}{21}R^4$	$\frac{18}{25}R^2$
$5s\rightarrow np\ ^1P$	$2R^0$	$-R^0$	$-\frac{1}{3}R^1$	$\frac{2}{3}R^1$
$5s\rightarrow ns\ ^1S$	$2R^0$	$-R^0$	$-R^0$	$2R^0$
$5s\rightarrow nd\ ^1D$	$2R^0$	$-R^0$	$-\frac{1}{5}R^2$	$\frac{2}{5}R^2$

$$\langle nl \mid V^N \mid n'l\rangle=(\mathrm{a})+(\mathrm{c})\ . \tag{A1}$$

(a) and (c) can be read in Table I for the different channels involved. In contrast with the ground state, the self-interaction terms in Figs. 13(a) and 13(c) do not cancel so that an excited electron interacts with N other electrons (in the case presented in Fig. 13, $N=6$ is the number of outer p electrons). A more "physical" single-particle potential for the excited state can be built by eliminating these self-interaction terms. This potential (V^{N-1}) is defined

$$\langle nl \mid V^{N-1} \mid n'l\rangle=(\mathrm{a})+(b_0)+(\mathrm{c})+1/N\ (\mathrm{d})\ . \tag{A2}$$

Again, (a), (b_0) [monopole part of (b)], (c) and (d) are indicated in Table I for the intermediate and final excited states of the two-photon transition. In this way, the self-interaction parts of Figs. 13(a) and 13(c) are approximately canceled (in average), respectively, by (b_0) and $1/N$ [(d)]. The remaining intrachannel interaction is then equal to $(b_2)+(N-1)/N$ [(d)], and it can be treated, for example, by the RPAE. The approximation that we have used in the calculation of the two-photon ionization cross section of xenon for the intermediate states (ns,nd) is defined as follows:

$$\langle nl \mid V \mid n'l\rangle=(\mathrm{a})+(\mathrm{b})+(\mathrm{c})\ . \tag{A3}$$

The complete direct intrachannel interaction (ladder diagrams) is included in the zeroth-order approximation. On the other hand, the self-interaction term in Fig. 13(c) is not canceled and the remaining intrachannel interaction is (d). The reason for which the exchange self-interaction is not removed is due to a bad numerical cancellation of the self-interaction in ground-state correlation diagrams represented in Figs. 13(e) and 13(f). The sum of the contribution of these diagrams [(e)+(f)] is closer to (f) than to $(N-1)/N$(f). Treating the forward- and backward-propagating bubbles on the same footing, it is then a better approximation to keep the full interaction (d) and (f) in the RPA expansion [neglecting (e)] and therefore not remove the exchange self-interaction in the potential.

The main difference between an RPAE calculation based upon a V^{N-1} potential defined in Eq. (A2) and an RPA calculation based upon this potential V [Eq. (A3)] is that in the latter case, interchannel ladder diagrams are not included. However, we have evaluated these diagrams and found that their contribution is negligible compared to interchannel bubble diagrams.

Finally, we may choose to include completely the intrachannel interaction in the zeroth-order approximation. The V^{N-1} HF-LS potential defined by

$$\langle nl \mid V^{N-1}LS \mid n'l\rangle=(\mathrm{a})+(\mathrm{b})+(\mathrm{c})+(\mathrm{d}) \tag{A4}$$

accounts for the polarization of the shell in which an electron-hole pair has been created. The infinite sum of forward-propagating bubble and ladder diagrams [called Tamm-Dancoff approximation with exchange (TDAE)] is included in the zeroth-order approximation and most of the dynamics of the excited system is then "hidden" in the basis set. Note, however, that, compared to an RPAE calculation, neither the interchannel interaction, describing, for example, the mixing of the $5p\rightarrow np$ and $5p\rightarrow ns$ channels, nor the ground-state correlation diagrams or more generally any diagram involving a double excitation are included in the V^{N-1} HF-LS potential.

[1] A. L'Huillier, L. A. Lompré, G. Mainfray, and C. Manus, Phys. Rev. A **27**, 2503 (1983); J. Phys. B **16**, 1363 (1983).

[2] A. L'Huillier, Comments At. Mol. Phys. **18**, 289 (1986).

[3] T. S. Luk, U. Johann, H. Egger, H. Pummer, and C. K. Rhodes, Phys. Rev. A **32**, 214 (1985).

[4] C. K. Rhodes, Science **229**, 1345 (1985).

[5] S. L. Chin, F. Yergeau, and P. Lavigne, J. Phys. B **20**, 723 (1987).

[6] For a comprehensive review, see M. Crance, Phys. Rep. **144**, 117 (1987).

[7] N. B. Delone, N. B. Suran, and B. A. Zon, in *Multiphoton Ionization of Atoms*, edited by S. L. Chin and P. Lambropoulos (Academic, New York, 1984), p. 235; D. Feldmann, H. J. Krautwald, and K. H. Welge, *ibid.*, p. 223.

[8] P. Agostini and G. Petite, J. Phys. B **17**, L811 (1984); Phys. Rev. A **32**, 3800 (1985).

[9] J. L. Dexter, S. M. Jaffe, and T. F. Gallagher, J. Phys. B **10**, L735 (1985).

[10] See, e.g., L. A. Lompré, A. L'Huillier, G. Mainfray, and C. Manus, J. Opt. Soc. Am. B **2**, 1906 (1985); H. J. Humpert, H. Schwier, R. Hippler, and H. O. Lutz, Phys. Rev. A **32**, 3787 (1985); P. H. Bucksbaum, M. Bashkansky, R. R. Freeman, and T. J. McIlrath, Phys. Rev. Lett. **56**, 2590 (1986); F. Yergeau, G. Petite, and P. Agostini, J. Phys B **19**, L663 (1986).

[11] C. K. Rhodes, Phys. Scr. T **17**, 193 (1987).

[12] X. D. Mu, T. Aberg, A. Blomberg, and B. Crasemann, Phys.

Rev. Lett. **56**, 1090 (1986).
[13]M. Crance, J. Phys. B **17**, 3503 (1984); **17**, 4333 (1984); **17**, L635 (1984); **18**, L155 (1985).
[14]S. Geltman, Phys. Rev. Lett. **54**, 1090 (1985); J. Zakrewski, J. Phys. B **19**, L315 (1986).
[15]H. Egger, U. Johann, T. S. Luk, and C. K. Rhodes, J. Opt. Soc. Am. B **3**, 901 (1986).
[16]K. Boyer and C. K. Rhodes, Phys. Rev. Lett. **54**, 1490 (1985).
[17]A. Szöke and C. K. Rhodes, Phys. Rev. Lett. **56**, 720 (1986).
[18]G. Petite and P. Agostini, J. Phys. (Paris) **47**, 795 (1986).
[19]U. Johann, T. S. Luk, H. Egger, and C. K. Rhodes, Phys. Rev. A **34**, 1084 (1986).
[20]P. Lambropoulos, Phys. Rev. Lett. **55**, 2141 (1985).
[21]G. Wendin, in *New Trends in Atomic Physic,* 1982 Les Houches Lectures, edited by G. Grynberg and R. Stora (Elsevier, New York, 1984) and references therein.
[22]G. Wendin, Comments At. Mol. Phys. **17**, 115 (1986); Phys. Rev. Lett. **53**, 724 (1984).
[23]A. F. Starace, Appl. Opt. **19**, 4051 (1980); *Corpuscles and Radiation in Matter I,* Vol. 31 of *Handbuch der Physik,* edited by W. Melhorn (Springer-Verlag, Berlin, 1982), p. 1.
[24]M. Ya Amusia and N. A. Cherepkov, Case Stud. At. Phys. **5**, 47 (1975); M. Ya Amusia, Adv. At. Mol. Phys. **17**, 1 (1981); Appl. Opt. **19**, 4042 (1980).
[25]H. P. Kelly, in *Atomic Physics 8,* edited by I. Lindgren, A. Rosen, and S. Svanberg (Plenum, New York, 1983), p. 305.
[26]A. Zangwill and P. Soven, Phys. Rev. Lett. **45**, 204 (1980); Phys. Rev. A **21**, 1561 (1980).
[27]G. A. Victor, Proc. Phys. Soc. London **91**, 825 (1967); B. Ritchie, Phys. Rev. A **16**, 2080 (1977).
[28]A. L'Huillier, L. Jönsson, and G. Wendin, Phys. Rev. A **33**, 3938 (1986).
[29]See also M. Crance and M. Aymar, J. Phys. (Paris) **46**, 1887 (1985), for a calculation of double ionization of He; M. Aymar and M. Crance, J. Phys. B **13**, 2527 (1980) and references therein for multiphoton ionization of metastable He.
[30]Y. S. Kim and P. Lambropoulos, Phys. Rev. A **29**, 3159 (1984).
[31]X. Tang and P. Lambropoulos, Phys. Rev. Lett. **58**, 108 (1987).
[32]M. S. Pindzola and H. P. Kelly, Phys. Rev. A **1**, 1543 (1975).
[33]R. Moccia, N. K. Rahman, and A. Rizzo, J. Phys. B **16**, 2737 (1983).
[34]E. J. McGuire, Phys. Rev. A **24**, 835 (1981).
[35]P. Gangopadhyay, X. Tang, P. Lambropoulos, and R. Shakeshaft, Phys. Rev. A **34**, 2998 (1986).
[36]A. F. Starace and T. F. Jiang, Phys. Rev. A **36**, 1705 (1987).
[37]A. Zangwill, J. Chem. Phys. **78**, 5926 (1983).
[38]K. R. Subbaswamy and G. D. Mahan, J. Chem. Phys. **84**, 3317 (1986); G. Senatore and K. R. Subbaswamy, Phys. Rev. A **34**, 3619 (1986).
[39]G. Wendin, L. Jönsson, and A. L'Huillier, Phys. Rev. Lett. **56**, 1241 (1986).
[40]A. L'Huillier and G. Wendin, J. Phys B **20**, L37 (1987).
[41]G. Wendin, L. Jönsson, and A. L'Huillier, J. Opt. Soc. Am. **4**, 833 (1987).
[42]G. Wendin, in *Giant Resonances in Atoms, Molecules and Solids, 1986 Les Houches Lectures,* Vol. 151 of *NATO Advanced Study Institute, Series B: Physics,* edited by J. P. Connerade, J. M. Esteva, and R. C. Karnatak (Plenum, New York, 1987), p. 171.
[43]G. Wendin, J. Phys. B **5**, 110 (1972); **6**, 42 (1973).
[44]M. Aymar and M. Crance, J. Phys. B **13**, L287 (1980).
[45]A. W. McCown, M. N. Ediger, and J. G. Eden, Phys. Rev. A **26**, 3318 (1982).